Chapter 2
Analysis of Solar Radiation Time Series

Abstract In this chapter, various kinds of analysis are performed by using solar radiation time series recorded at 12 stations of the NREL database. Analysis are devoted to infer some basic properties, such as stationarity, autocorrelation, and the embedding phase-space dimension. These features will be considered in the rest of the book to implement short-term forecasting models and perform the clustering of solar radiation daily patterns. Furthermore, others kinds of analysis are carried out, such as the fractal and multifractal analysis and estimation of Lyapunov exponents, in order to clarify more deeply the nature of solar radiation time series.

2.1 Energy from the Sun

The Sun is certainly the main source of renewable energy. Just to have an idea it is possible to say that the Sun delivers toward the surface of the terrestrial hemisphere exposed a power exceeding 50 thousand Tera Watt which is about 10 thousand times the energy used all over the world [1]. A part of this energy reaches the outer part of the Earth's atmosphere with an average irradiance of about 1367 W/m^2, a value which varies as a function of the Earth-to-Sun distance and of the solar activity. The problem of estimating the global horizontal solar radiation $GHI(h, d)$, for any hour h of a day d of the year, at any site, has been addressed in literature by several authors such as [2]. It depends on a quite large number of parameters which, roughly speaking, can be summarized as follows: the distance from the sun, the duration of the daily sunlight period, the inclinations of solar rays to the horizon, the transparency of the atmosphere toward heat radiation and the output of solar radiation. Some of these factors are connected with mechanical parameters which describes the revolution of Earth around the Sun and on the Earth spinning about itself. Others factors depend on the properties of the atmosphere and are stochastic in nature, such as the cloud cover features (size, speed, and number) and the degree of pollution.

When passing through the atmosphere, the solar radiation decreases in intensity because it is partially reflected and absorbed, mainly by the water vapor and others atmospheric gases. The radiation which passes through is partially diffused by the air and by the solid particles suspended in the air. Therefore, the radiation falling

L. Fortuna et al., *Nonlinear Modeling of Solar Radiation and Wind Speed Time Series*, SpringerBriefs in Energy, DOI 10.1007/978-3-319-38764-2_2

on a horizontal surface is constituted by a direct radiation, associated to the direct irradiance on the surface, by a diffuse radiation and by a radiation reflected on a given surface by the ground and by the surrounding environment. In winter, when the sky is usually overcast, the diffuse component is greater than the direct one.

2.2 The Solar Radiation Data Set

The data set considered in this book consists of hourly average time series recorded at 12 stations stored in the USA National Solar Radiation Database managed by the NREL (National Renewable Energy Laboratory). Data of this database was recorded from 1999 to 2005 and can be freely download as described in Appendix A.2. The 12 stations were selected based on two criteria: the quality of time series and the need to ensure the necessary diversification of meteo-climatic conditions. The 12 selected stations are listed in Table 2.1. More detailed information about these and others recording stations of the National Solar Radiation Database can be found in [3]. Analysis of solar radiation time series has been addressed in literature by various authors such as [4–6]. Nevertheless, as the available results are sometimes fragmented, in this section it is provided a picture as comprehensive as possible of features of this kind of time series. Analysis performed refer to aspects such as stationarity, power spectrum, autocorrelation, fractal, and embedding state-space dimension. According with the basic knowledge about solar radiation, Fig. 2.1 shows that the considered kinds of time series are fluctuating at any time scale. Indeed, in the Figure a time series is shown at hourly, daily, monthly, and yearly time scales. Fluctuations observed in solar radiation time series is a feature shared with other meteorological time series, such as wind speed. These fluctuations are superimposed

Table 2.1 Coordinates of the 12 solar radiation recording stations

stationID	Description	*Lat*	*Lon*	*Elev*	*UTC*
690140	El Toro MCAS (CA)	33.667	−117.733	116	−8
690150	Twenty-nine Palms (CA)	34.3	116.167	626	−8
722020	Miami Int AP (FL)	25.817	−80.3	11	−5
722350	Jackson Int AP (MS)	32.317	−90.083	94	−6
722636	Dalhart Municipal AP (TX)	36.017	−102.55	1216	−6
723647	Albuquerque Double (NM)	35.133	−106.783	1779	−7
724776	Moab Canionlands(UT)	38.58	−109.54	1000	−7
725033	New York Central PRK (NY)	40.783	−73.967	40	−5
725090	Boston Int AP, (MA)	42.367	−71.017	6	−5
726055	Pease Int Tradepor (NH)	43.083	−70.817	31	−5
726130	Mount Washington (NH)	44.267	−71.3	1910	−5
726590	Aberdeen Regional AP (SD)	45.45	−98.417	398	−6

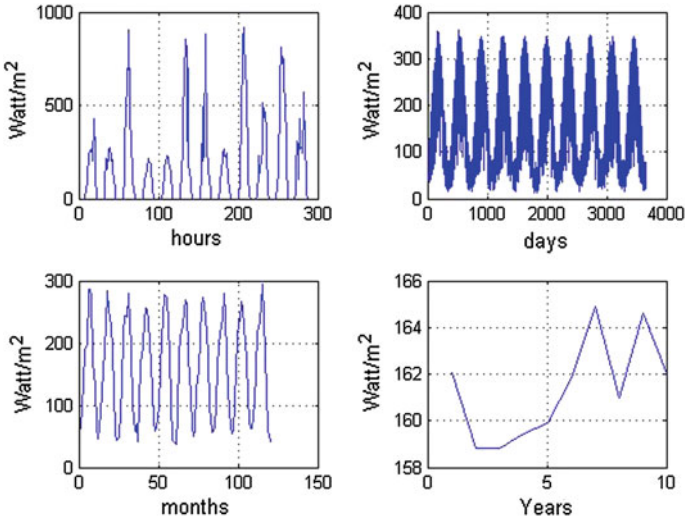

Fig. 2.1 Solar radiation time series at hourly, daily, monthly, yearly scale, respectively

with deterministic variations due to the Earth spinning around itself and to the revolution of Earth around the Sun. The Earth spinning determines the typical bell shape curves that are visible at hourly scale, while the revolution around the Sun determines the fluctuations that are visible at monthly scales. However, fluctuations occur also from year to year, as shown in lower rightmost sub Fig. 2.1.

2.2.1 Stationarity Analysis

One of the preliminary issues that one would like to know is if solar radiation time series are stationary. To this purpose, usually, available tests are based on the search for existent of a *unit root*, such as the Dicky–Fuller and the Phillips–Perron tests (see the *adftest* and the *pptest* functions, listed in Appendix A.1). The application of these tests indicate that the null-hypothesis, i.e., the considered time series are nonstationary, is false.

Another approach to search for nonstationary evidences in time series is that of using recurrent plots (see the function *recurr* in Appendix A.1). Such a kind of plots obtained from hourly average solar radiation time series, for two different embedding dimensions, are shown in Fig. 2.2. Since it is known that in an ergodic situation, the dots of a recurrent plot should cover, on average, the plane uniformly, whereas nonstationarity expresses itself by an overall tendency of dots to be close to the diagonal, it is possible to conclude that there are not evidences that solar radiation time series are nonstationary, at least for time intervals of 10 years, as for the data set considered in this book.

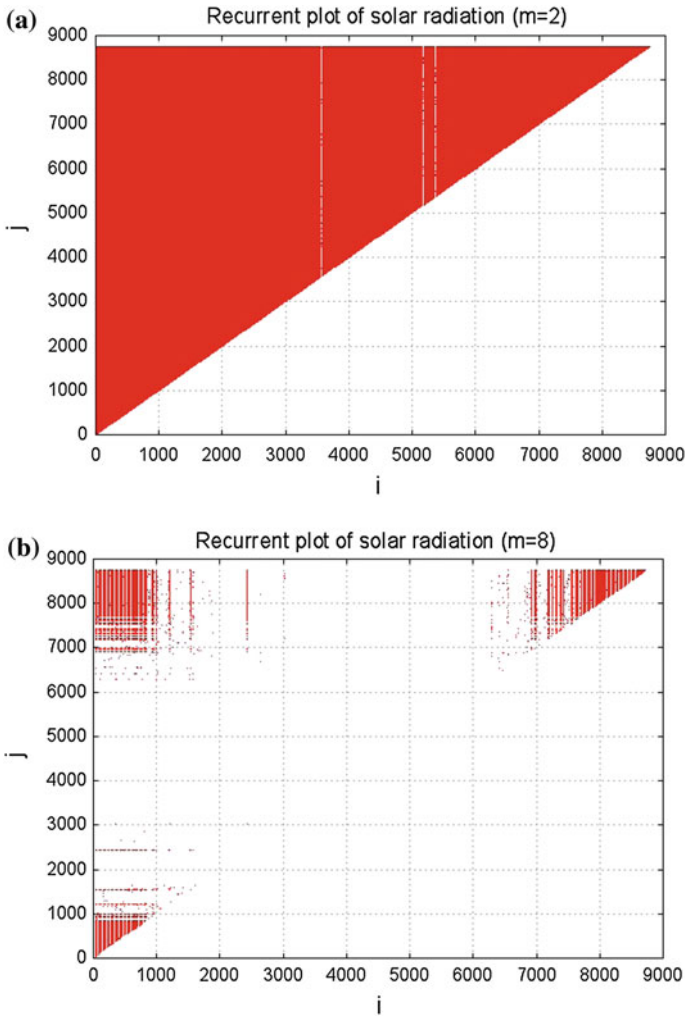

Fig. 2.2 Recurrent plots of solar radiation for two different embedding dimensions. **a** m = 2. **b** m = 8

2.2.2 *Autocorrelation and Mutual Information*

The autocorrelation functions computed for hourly and daily average solar radiation time series are reported in Fig. 2.3. As it is possible to see the autocorrelation function of hourly average solar radiation is strongly periodic with period 24 h, due to the marked daily component, already pointed out (see the upper leftmost Fig. 2.1). Furthermore, the autocorrelation function computed at hourly scale decays at values lower than 0.37, the so-called correlation time τ_c, in about 5 h. At daily scale the

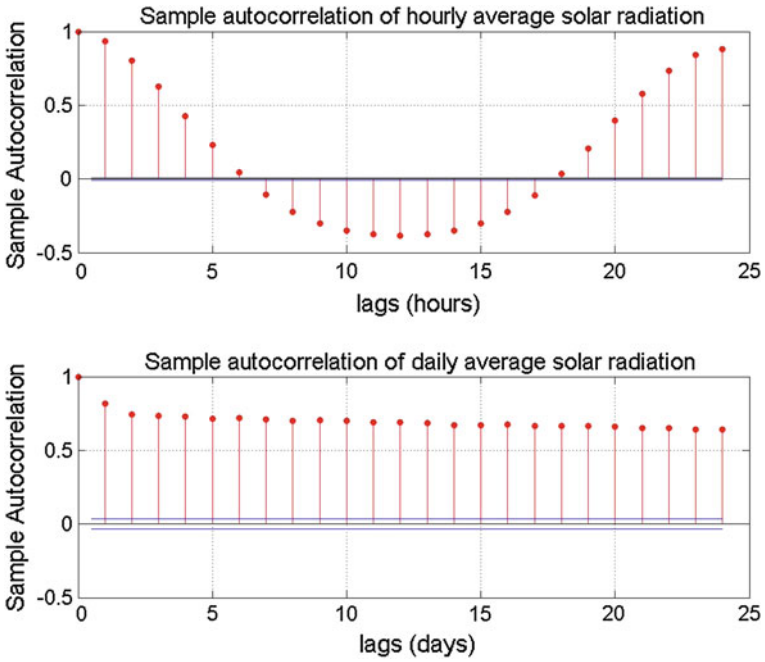

Fig. 2.3 Autocorrelation of typical hourly and daily average solar radiation time series

autocorrelation decays very slowly, which means that daily average solar radiation time series are long-range correlated.

Since the autocorrelation is a linear feature of time series, while it is reasonable that nonlinear processes are involved with solar radiation, it is useful to estimate also the mutual information, as shown in Fig. 2.4. A popular rule, referred to as the first minimum criterion, usually considered in evaluating the mutual information, is that two samples can be considered statistical independent if they are delayed by a number of samples equal to the time needed for the mutual information to reach the first minimum. By using this criterion at hourly scale two samples can be considered statistically independent if delayed by about six lags, while at daily scale if delayed about one lag. Thus, the analysis of the mutual information essentially confirms the results gathered by the autocorrelation function at hourly scale, but provides some more insight at daily scale.

2.2.3 Power Spectra

The typical power spectra of hourly and daily solar radiation time series are shown in Fig. 2.5. It is possible to observe that at hourly scale there are marked components with periods:

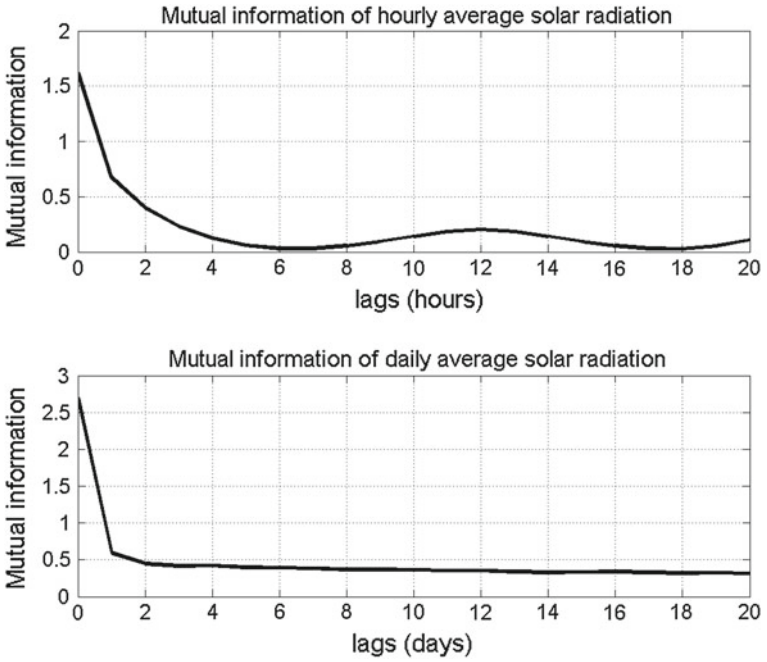

Fig. 2.4 Mutual information of typical hourly and daily average solar radiation time series

$T_1 = 1/0.0001143 \simeq 8748\,\text{h} \simeq 1\,\text{year}$,
$T_2 = 1/0.04167 \simeq 24\,\text{h}$.

The others components of the spectrum computed at hourly scale corresponding to periods of 12 h, 6 h etc., are well-known effects of the considered fast Fourier transform (FFT) computing algorithm. At daily scale only one marked component is evident, corresponding to a period of $T_3 = 1/0.002743 \simeq 365$ days, i.e., 1 year.

The absolute values of the power spectra slopes computed for all the stations considered in this book are reported in Table 2.2. We obtained that the mean slope of hourly and daily time series is about 1.05 and 0.67 respectively. The difference among these slopes can be easily explained bearing in mind that daily average solar radiation time series are less autocorrelated than the corresponding hourly average, and thus, more similar to a white noise. However, both hourly and daily average time series can be classified as $1/f$ noises (see Sect. 1.8).

2.2.4 Hurst Exponent and Fractal Dimension

The Hurst exponent of hourly average time series obtained by using the detrended fluctuation algorithm (DFA) [7], and the fractal dimension, computed by using the

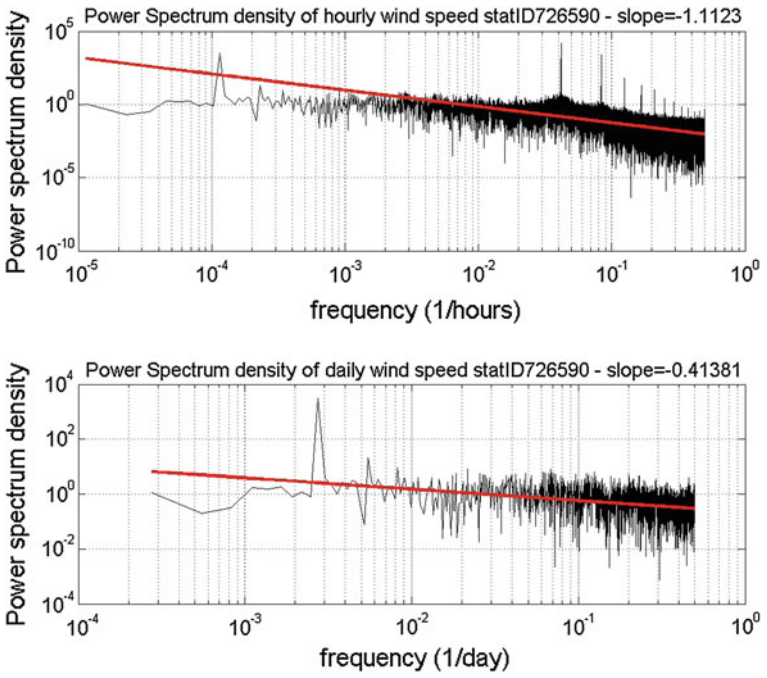

Fig. 2.5 Power spectrum densities of hourly and daily average solar radiation time series at the station ID 726590

Table 2.2 Absolute slopes of power spectra of hourly (column 2) and daily (column 3) solar radiation averages, Hurst exponent (column 4), and box dimension (column 5) of the hourly solar radiation time series at the 12 considered stations

stationID	$\beta(hourly)$	$\beta(daily)$	H	D
690140	1.1651	0.8443	0.7614	1.4603
690150	0.8992	0.8928	0.7806	1.4601
722020	0.8236	0.7104	0.6740	1.4642
722350	1.0973	0.6962	0.7326	1.4599
722636	1.1147	0.6664	0.7655	1.4592
723647	0.9262	0.6506	0.7549	1.4601
724776	0.8753	0.6454	0.7965	1.4638
725033	1.1706	0.5538	0.7661	1.4618
725090	1.2606	0.5329	0.7740	1.4603
726055	1.1999	0.5682	0.7742	1.4597
726130	1.0360	0.6198	0.7951	1.4630
726590	1.0932	0.6837	0.8258	1.4604

boxcounting algorithm [8] at the considered stations are shown in Table 2.2. It is possible to see that, H and D, gives on average $H = 0.77$ and $D = 1.46$. These values clearly point out the fractal nature of solar radiation time series. In particular, the Hurst exponent indicates that they are positive long-range correlated since $0.5 < H < 1$ (see Sect. 1.9.2).

2.2.5 Multifractal Analysis of Solar Radiation

One of the techniques proposed in the literature to deal with multifractal is the multifractal detrended fluctuation analysis (MFDFA) [9] developed as the extension of the DFA. In the framework of MFDFA analysis a generalized Hurst exponent $H(q)$ is defined, depending on the local fluctuation exponent q. Furthermore, it is defined the so-called multifractal spectrum (also referred to as singularity spectrum). According with [6], who recognized the multifractal nature of solar radiation time series, we report some further evidences obtained by performing the multifractal analysis at some of the stations listed in Table 2.1. The generalized Hurst exponents and the corresponding multifractal spectrum of these stations are reported in Fig. 2.6a and b, respectively. Figure 2.6a clearly shows a marked dependence of $H(q)$ on q, thus confirming the multifractal nature of solar radiation time series. In order to interpret the multifractal spectrum reported in Fig. 2.6b it is to bearing in mind that it has an asymmetric bell shape with the maximum obtained for $q = 0$. The multifractal spectrum will have a long left tail when the time series have a multifractal structure that is insensitive to the local fluctuations with small magnitude. In contrast, the multifractal spectrum will have a long right tail when the time series have a multifractal structure that is insensitive to the local fluctuations with large magnitudes. Figure 2.6b shows that the five stations exhibit right tails, i.e., the spectra are left truncated, which simply means that while large fluctuation scales within a limited range of exponents $\alpha \in [0.66, 0.7]$, the small fluctuation scales following a wider range of exponents $\alpha \in [0.7, 1]$.

2.2.6 Estimation of the Embedding Dimension

In order to determine the embedding dimension d of the dynamical system underlying solar radiation time series, the fraction of false nearest neighbors was computed, as shown for instance in Fig. 2.7. The Figure shows that the fraction of false nearest neighbors decays very slowly with the embedding dimension, without reaching the zero value in the range $d \in [1, 30]$. However, it seems that the curve reaches a steady state for $d \geq 24$. While the fact that a zero value is not reached can be interpreted as the effect of noise in the considered time series, the value $d = 24$ can be justified bearing in mind that hourly average solar radiation time series exhibits a strong daily component, i.e., with period 24 h.

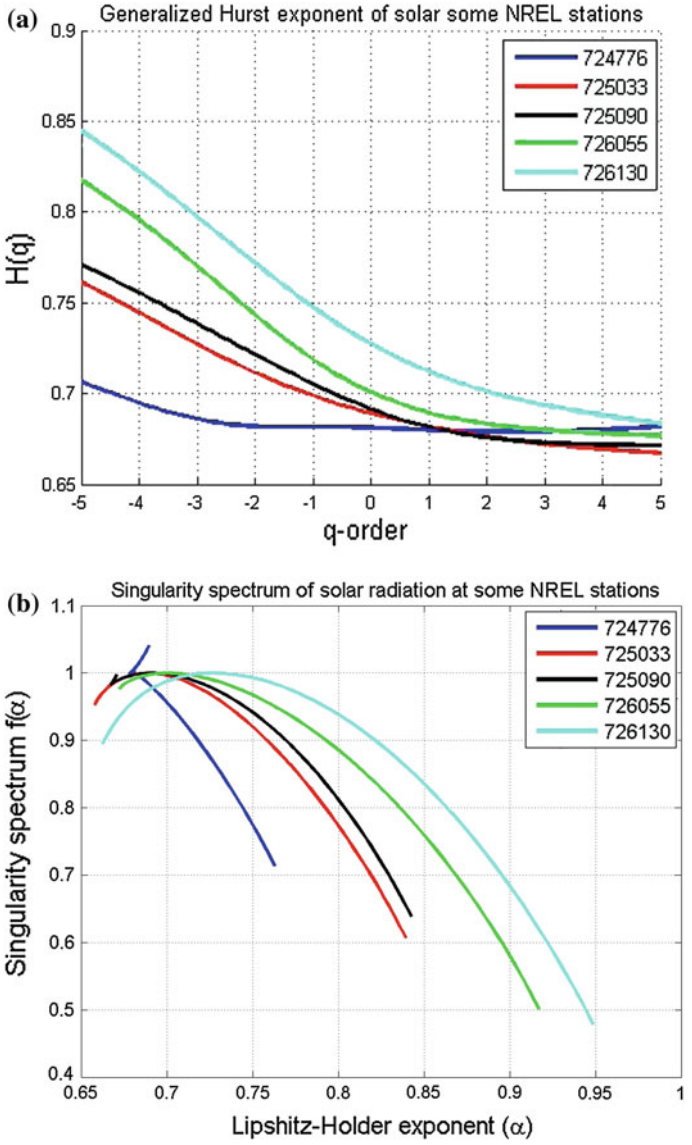

Fig. 2.6 Generalized Hurst exponent and singularity spectrum at some of the considered solar radiation recording stations. **a** Generalized Hurst exponent. **b** Singularity spectrum

2.2.7 Maximal Lyapunov Exponent

As mentioned in Sect. 1.12, a bounded dynamical system with a positive Lyapunov exponent is chaotic, and the so-called maximal exponent describes the average rate at which predictability is lost (see [10]). Results obtained computing the maximal Lya-

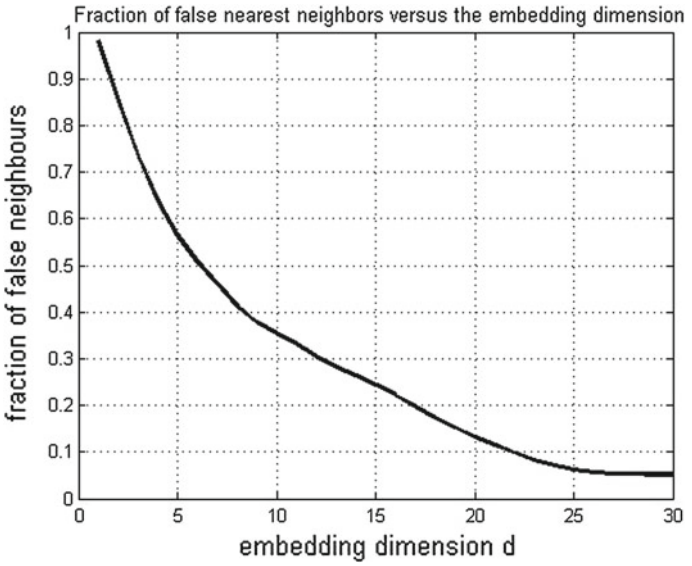

Fig. 2.7 Fraction of false nearest neighbors of solar radiation versus the embedding dimension d

punov exponent of hourly average time series recorded at the considered stations, by using the *lyap_k* function indicate the existence of positive maximal exponents in the range [0.6, 1]. This result would indicate that the hourly average solar radiation time series are chaotic. However, since this result if confirmed, would have some interesting implications, it is given here as a work in progress and further investigations are needed.

2.3 Conclusions

Analysis presented in this Chapter, performed on both hourly and daily average solar radiation time series allow to draw some conclusions about their nature. Stationary analysis, carried out by different approaches, has not pointed out evidences that they are nonstationary, at least for time intervals of 10 years, which is the largest considered in this study. The power spectrum analysis has shown that the slopes of the solar radiation time series power spectra are in the range [0.5, 1.5], which means that solar radiation time series belong to the wide class of $1/f$ noise. Correlation analysis, carried out by using linear and non linear approaches, pointed out that solar radiation time series exhibits a correlation time of about $\tau_c = 5$ lags at hourly time scale and of about $\tau_c = 1$ lag at daily scale, which means that prediction models, based on autocorrelation, can be reliable for short horizons only. Fractal analysis pointed out that these kind of time series are fractal exhibiting, on average, fractal

dimension $D = 1.46$ and Hurst exponent of $H = 0.77$. Furthermore, the multifractal detrended fluctuation analysis (MFDFA) has pointed out that solar radiation time series are multifractal. analysis carried out in order to see if there are evidences of deterministic chaos, as suggested by the presence of at least a positive exponent in the range [0.6, 1], needs further investigations, since as well known the computation of Lyapunov exponents from time series is rather difficult and may have some drawbacks.

References

1. AAVV, Photovoltaic plants, ABB Technical Application Paper N. 10, 1–124
2. S. Kaplanis, E. Kaplani, A model to predict expected mean and stochastic hourly global solar radiation values. Renew. Energy **32**, 1414–1425 (2007)
3. S. Wilcox, National Solar Radiation Database 1991-2010 Update—Users Manual, Technical Report NREL/TP-5500-54824, 1–479, 2012. ftp://ftp.ncdc.noaa.gov/pub/data/nsrdb-solar/documentation-2010/
4. A. Maafi, S. Harrouni, Preliminary results of the fractal classification of daily solar irradiance. Solar Energy **75**, 53–61 (2003)
5. S. Harrouni, A. Guessoum, Using fractal dimension to quantify long-range persistence in global solar radiation. Chaos Solitons Fractals **41**, 1520–1530 (2009)
6. Z. Zeng, H. Yang, R. Zhao, J. Meng, Nonlinear characteristics of observed solar radiation data. Solar Energy **87**, 204–218 (2013)
7. R. Weron, Estimating long range dependence finite sample properties and confidence intervals. Physica A **312**, 285–299 (2002)
8. N. Sarkar, B.B. Chaudhuri, An efficient differential box-counting approach to compute fractal dimension of image. IEEE Trans. Syst. Man Cybern. **24**, 115–120 (1994)
9. J.W. Kantelhardt, S.A. Zschiegner, E. Koscielny-Bunde, A. Bunde, S. Havlin, H.E. Stanley, Multifractal detrended fluctuation analysis of nonstationary time series. Physica A **87–114**, 316 (2002)
10. J.C. Sprott, *Chaos and Time-Series Analysis* (2003)

http://www.springer.com/978-3-319-38763-5

Nonlinear Modeling of Solar Radiation and Wind Speed Time Series

Fortuna, L.; Nunnari, G.; Nunnari, S.

2016, XV, 98 p. 57 illus., 49 illus. in color. With online files/update., Softcover
ISBN: 978-3-319-38763-5